Design of Optical Full Encoders/Decoders for Code-Based Photonic Routers

Gabriella Cincotti, *Member, IEEE, Member, OSA*

***Abstract*—This paper demonstrates that standard multiplexers as generalized Mach–Zehnder interferometers or waveguide grating routers can be designed to generate/process a set of orthogonal optical codes (OCs) with very high-correlation performances. The same device can be used at the ingress node of a generalized multiprotocol label switching network to generate the photonic labels and at each routing node to perform all the correlations simultaneously. To enhance the code cardinality, without increasing the code length, this paper shows that it is possible to use the proposed encoder/decoder architectures to generate/process multidimensional OCs.**

***Index Terms*—Codecs, coding, communication system routing, decoding, optical correlators.**

THE MOST promising trend of future optical networking envisages a two-layer architecture with an upper data layer devoted to service integration on Internet protocol (IP) and a lower physical layer devoted to flexible optical transport. It is widely recognized that a single control plane that governs both layers is the solution to supporting the exponential growth of internet traffic as well as to satisfying emerging requests for new dynamic services, like *bandwidth on demand* or optical *virtual private networks*. This is the concept upon which generalized multiprotocol label switching (GMPLS) and automatically switched optical networks (ASONs) are based. ASONs provide new functionalities to optical networks, such as a dynamic setup of optical connections, fast and efficient restoration mechanisms, and solutions for automatic topology discovery [1]–[4]. GMPLS introduces distributed intelligence in multilayer networks, and overlays an optical packet/burst switched network to facilitate traffic engineering and reserve bandwidth for traffic flows with different quality of service (QoS) [5]–[13]. Therefore, GMPLS combines the flexibility of IP with the benefits of connection-oriented protocols [14], providing virtual links in the optical network: at each label edge routing (LER) node, standard IP routing is suspended, and a label is inserted in front of each data packet. At each label switch routing (LSR) node, the data packets are routed according to the label value and forwarded to the next hop with a new label value, as illustrated in Fig. 1.

The generation and recognition of GMPLS labels in the optical domain resolves the electronic router's bottleneck. According to GMPLS resource reservation protocol (RSVP) and constraint-based-routed label distribution protocol (CR-LDP), a generalized label is a time slot, a wavelength, or a fiber of a bundle; data packets are switched in time, frequency, and space domains, with a combined use of synchronous optical network/synchronous digital hierarchy (SONET/SDH) time-division multiplexing (TDM), wavelength-division multiplexing (WDM) techniques, and optical cross connects (OXCs). According to the natural hierarchy of label switch paths (LSPs), nodes with fiber switch-capable (FSC) interfaces are followed by nodes with lambda switch-capable (LSC) interfaces, followed by nodes with TDM-capable interfaces, followed by nodes with packet switch-capable (PSC) interfaces, which route electronic data packets as shown in Fig. 2 [5]. In current GMPLS network architectures, the LSP hierarchy is mandatory as the number of required labels is much larger (about one million per port) than the lambdas and TDM time slots (tens to hundreds) and parallel links between pairs of nodes (rarely more than ten) [5].

In standard GMPLS networks, WDM/TDM bandwidth allocation is from a small *discrete* set of values, whereas the LSP link bandwidth is not discrete: this shortcoming is often referred as the *granularity* issue of GMPLS [5], [15]. In addition, assigning a label at each fiber, lambda, and TDM channel is a serious concern, as well as the identification of the virtual path connections and the fault detection/isolation, because of the network management *complexity*. Finally, the open shortest path first/intermediate system to intermediate system (OSPF/IS-IS) routing protocol has to advertise the *availability* of optical resources in the network, such as physical connections or bandwidth on TDM/WDM links.

All of these shortcomings can be addressed, introducing a new dimension in ASON/GMPLS switching capability by photonic codes. Photonic routers that switch data streams according to optical codes (OCs) would enhance the *flexibility* of current ASON/GMPLS, solve the *label deficiency problem*, simplify the label distribution protocol, and enable a more efficient resource allocation and a faster bandwidth provisioning. Furthermore, the control planes of the data packet traffic and the optical network could act as *peers*, and this more complete integration between data and optical layers would greatly enhance the efficiency of network resources utilization. Management of optical networks can be performed more cost effectively by fully transparent OXCs, independent of wavelength and bit rate; furthermore, labels can be much more easily distributed according to standard protocols RSVP and CR-LDP, because they are not related to network resources, avoiding any conflict during the LSP setup. Finally, code-based photonic routers could also replace LSC routers, avoiding the use of tuneable laser sources, optical add/drop multiplexers (OADMs), and wavelength converters. In this case, WDM could be much more efficiently used

Manuscript received December 5, 2003; revised March 22, 2004.

The author is with the Department of Applied Electronics, University of Rome Tre, I-00146 Rome, Italy (e-mail: g.cincotti@uniroma3.it).

Digital Object Identifier 10.1109/JLT.2004.829190

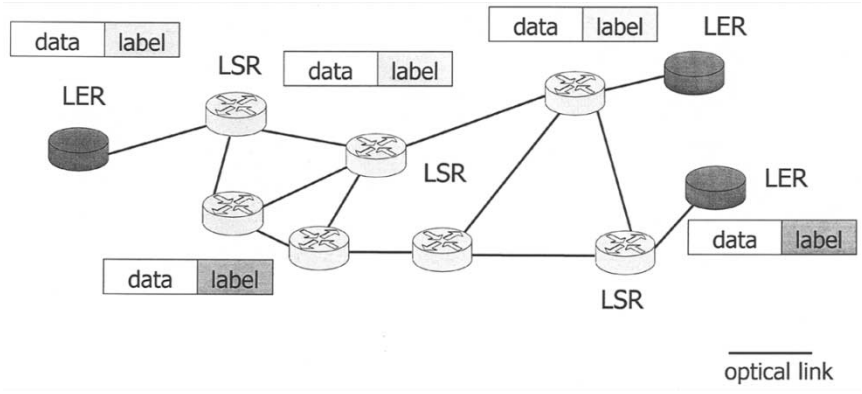

Fig. 1. Scheme of a GMPLS network. At each LER node, a label is inserted in front of the optical data packet, and at each LSR node the packet is routed according to the label value.

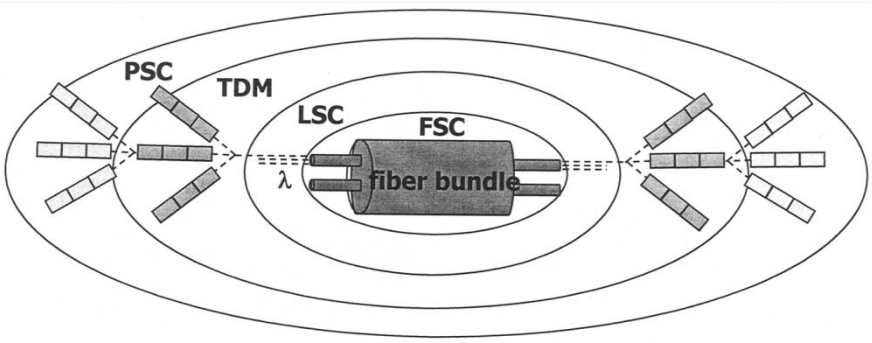

Fig. 2. LSP hierarchy in a GMPLS network. Nodes with FSC interfaces are followed by nodes with LSC interfaces, followed by nodes with TDM-capable interfaces, followed by nodes with PSC interfaces.

to transport (and not route) aggregated data streams in core networks.

A photonic IP router that processes labels in the optical domain can process about 10^{10} packets per second, whereas the processing speed of electrical IP routers is only 10^6 packets per second [17].

Kitayama and Wada developed very innovative architectures for code-based photonic routers, where each LSR node consists of an optical gate switch and a label processor [15]–[21]. The optical label processing is accomplished by splitting the incoming optical frame into as many copies as the entries in the address bank; N different all-optical correlators are employed to perform the correlations in parallel, and the detection of the autocorrelation peak reveals an exact match.

In a recent paper [22], a novel scheme for full encoders/decoders (E/D)s [23] has been presented that generate/process a set of N OCs simultaneously and can be advantageously used in GMPLS networks, as well as in optical-code-division multiple-access (OCDMA) networks [24], [25]. A tree of Mach–Zehnder interferometers (MZIs) with input and output symmetrical 3-dB couplers generates N orthogonal OCs and that the same device can be used to correlate N code sequences directly in the optical domain. It was remarked that the number N of the OCs coincides with the number of the code chips and that the E/D can generate/process only a certain set of all the possible combinations; however, all of the OCs are orthogonal. In addition, the analogy between the construction of the OC's sequences and a subband filtering process was evidenced, where a signal is analyzed by a bank of optical filters [26].

A full E/D has a single input and N outputs: at an ingress LER node of the GMPLS of Fig. 1, a short light pulse (that coincides with the label chip) is driven into the device input and N orthogonal labels are simultaneously generated. A single label is selected by an optical switch and is multiplexed at the head of a data packet, after an optical guard band that facilitates the label removal or swapping, as illustrated in Fig. 3(a). At every LSR node, the entire packet (label + data) is forwarded to the device input, and N correlation functions, with all the N entries of the table lookup, are obtained at its outputs: the autocorrelation peak (ACP) detected at one output reveals an exact match of the incoming label and the corresponding code, as depicted in Fig. 3(b). Therefore, the same device can be used at the each LER node to generate the OCs in the optical domain as well as at each LSR node to process the photonic labels.

To reduce the error sensitivity, it is necessary that the maximum cross-correlation peak (CCP) is much lower than the ACP, and we designed different E/D architectures to generate/process different signature sets [22]. For instance, we generated the full Hadamard code set that is characterized by ACP $= N^2$ and maximum CCP $= (N-1)^2$; for $N = 8$, the error sensitivity is CCP/ACP $= 0.77$. We also designed an optimal OC with a very high error rejection: these labels have ACP $= N^2$, but a much lower value of the CCP; for instance, for $N = 8$, the error sensitivity is CCP/ACP $= 0.107$ so that the error rejection is enhanced 86% with respect to the Hadamard codes.

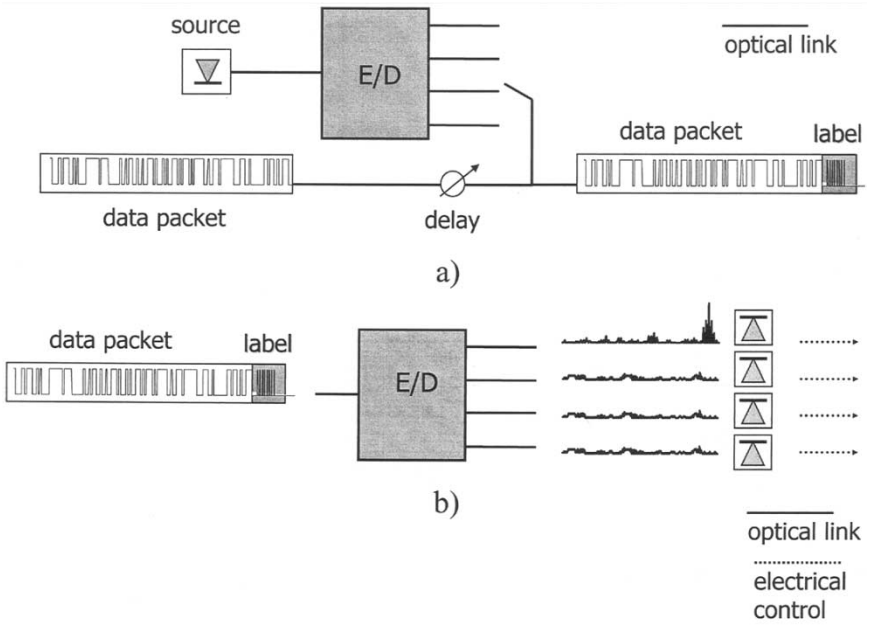

Fig. 3. (a) Label generation at LER nodes: A single optical pulse is driven into the E/D input and N orthogonal optical labels are generated, which are multiplexed at the head of the data packet. (b) Label recognition at LSR nodes: The entire packet (label + data) is forwarded to the device input, and N correlation functions are obtained at the N outputs: The ACP detected at one output reveals an exact match of the incoming label and the corresponding code in the lookup table.

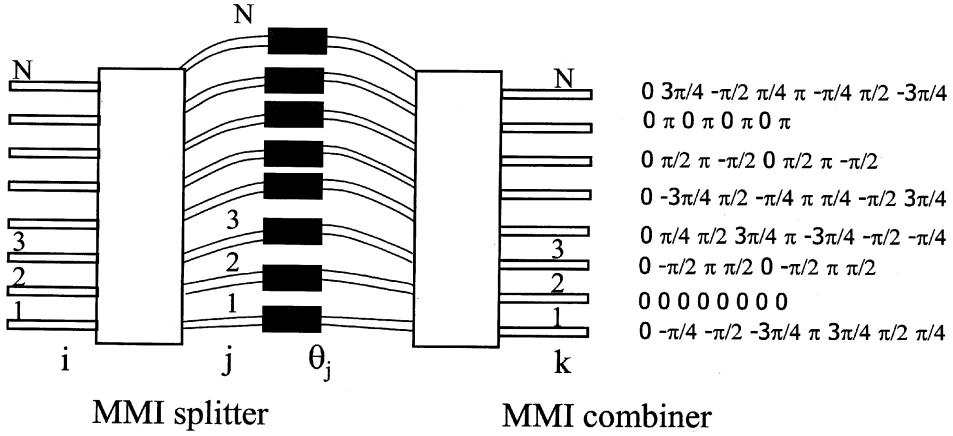

Fig. 4. GMZI configuration. The E/D is composed of two uniform MMI couplers with N inputs/outputs and a set of N delay lines with different lengths. i are the input ports, k the output ports, j the array arms, and θ_j the phase shifters values. In the right-hand side of the figure, the phase values of the OCs are reported.

The present paper demonstrates that the optimal codes from a tree of MZIs can be generated by a generalized MZI (GMZI) composed of two multimode interference (MMI) couplers, an array of N waveguides, and N optical phase shifters, as illustrated in Fig. 4, or with a waveguide grating router (WGR), which is shown in Fig. 5. Both devices are multiplexers that decompose the input signal into N frequency channels, but they can be designed also as full E/Ds: if a short chip pulse is driven into their inputs, as a set of orthogonal OCs are obtained at their outputs.

The design rules of an E/D with GMZI or WGR configurations are different from those of a frequency multiplexer: for instance, a multiplexer is usually designed to operate over N equally spaced wavelength channels, whereas it is necessary that the OC chips are equally spaced. The aim of this present paper is to furnish guidelines to design a full E/D using the architectures of Figs. 4 and 5.

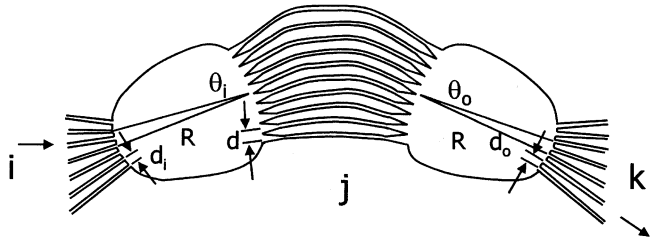

Fig. 5. WGR configuration. The E/D is composed of two slab couplers with N inputs/outputs and a set of N delay lines with different lengths. i are the input ports, k the output ports, and j the array arms. d is the pitch of the arrayed-waveguide grating (AWG), and d_i and d_o are the pitches of the input and output waveguide arrays, respectively. θ_i and θ_o are the diffraction angles in the input and output slabs, respectively, and R is the slab focal length.

The devices of Figs. 4 and 5 generate N orthogonal OCs, each of which is composed of N chips. Therefore, an increase

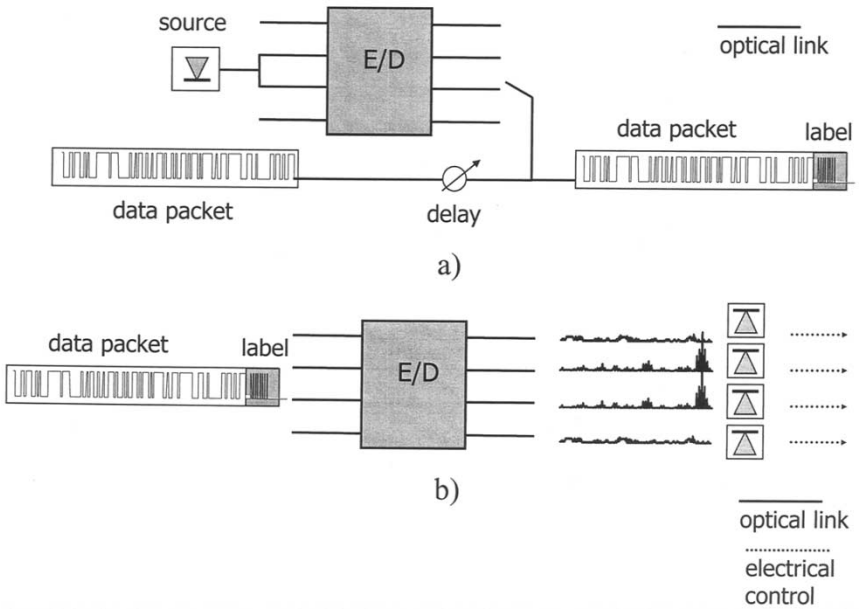

Fig. 6. (a) Label generation at LER nodes with a multidimensional E/D: n optical pulse are driven into the E/D inputs, and N orthogonal optical labels are generated, which are multiplexed at the head of the data packet. (b) Label recognition at LSR nodes with a multidimensional E/D: The entire packet (label + data) is forwarded to one of the device inputs, and N correlation functions are obtained at the N outputs. The n ACPs detected at the n outputs reveal an exact match of the incoming label and the corresponding code in the lookup table.

in the number N of the orthogonal labels, often termed as *code cardinality*, results in an increase of the label length and processing time. This paper shows that it is possible to increase the number of the labels without modifying their lengths, using multidimensional E/Ds, i.e., considering more than one input in the devices of Figs. 4 and 5. We call these devices as *multidimensional E/Ds*, in analogy to the time-spreading/wavelength-hopping optical E/Ds that generate two-dimensional (2-D) OCs in the time–frequency plane [27], [28]. However, in the present paper, a single frequency is considered, even though the extension to the case of multifrequency multidimensional OCs is quite immediate.

In Section III, it is shown that by driving $n \leq N$ optical pulses into the E/D inputs, N orthogonal OCs at their outputs are obtained, as depicted in Fig. 6(a). The code cardinality of multidimensional OCs depends on the number of the different combinations of the n inputs and is $\binom{N}{n}$, whereas the code length remains N. For instance, for $N = 8$ and with $n = 4$ input pulses, 70 different orghogonal labels can be generated, whereas for $N = 16$ and $n = 8$, 12 870 different labels can be built, solving the GMPLS label deficiency problem. In addition, the same device can be used to correlate all the multidimensional labels; in fact, if a label is driven into a device input, at the device outputs we measure n ACPs and $N - n$ cross-correlation signals [see Fig. 6(b)]. Therefore, an exact label matching is detected by measuring n ACPs, instead of a single ACP of a standard OC set.

I. GMZI Configuration

In literature, the multiplexer of Fig. 4 is referred to as *GMZI* or *GMZI phasar* [29] and has N inputs and N outputs. A standard E/D has only a single input so that the first MMI coupler can be either a $N \times N$ uniform power splitter or a $1 \times N$ nonuniform splitter [30]. In the present paper, we consider only the first case, as the layout of a GMZI with a nonuniform MMI splitter can be easily designed according to the following guidelines.

We use the same numbering direction for the input ports (i), the output ports (k), and the array arms (j). The E/D of Fig. 4 is symmetrical in the sense that input and output ports can be used interchangeably; in addition, owing to the reciprocity of the device, the impulse response $h_{ik}(t)$ from the input i to the output k coincides with the impulse response $h_{i'k'}(t)$ from the input i' to the output k', if $i' = k$ and $k' = i$.

A uniform MMI coupler is a waveguide designed to support a large number of modes on the transverse direction and to be monomode along the vertical axis, which is connected to N incoming and N outgoing single-mode waveguides (see Fig. 7). Due to the self-imaging property of multimode waveguides, a field distribution at any of the inputs is reproduced at the output plane in N images, which have equal amplitudes and different phases. To generate N images, it is necessary that the MMI coupler has a length $L_c = 3ML_\pi/N$ [31], where M and N are any positive integers without a common divisor and

$$L_\pi = \frac{\pi}{\beta_0 - \beta_1} = \frac{4n_g W_e^2}{3\lambda}. \tag{1}$$

Here, β_0 and β_1 are the propagation constants of the zeroth- and first-order modes, respectively, n_g the (effective) refractive index, and λ the free-space wavelength [31]. W_e is the effective width of the fundamental transverse mode, which is slightly larger than the actual slab width W, to take the lateral penetration depth of each mode field into account; for high-contrast waveguides, one can assume $W_e \simeq W$. In the most number of practical applications, integrated optical devices should be as short as possible, and MMI couplers are usually designed with $M = 1$. Fig. 7 shows the schematic of an $N \times N$ MMI

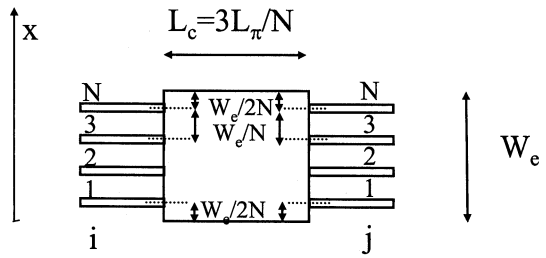

Fig. 7. Schematic of a uniform $N \times N$ MMI coupler. i and j are the input and output ports, respectively. L_c and W_e are the length and the effective width of the MMI coupler.

coupler; the incoming and outgoing waveguides are placed at equally spaced positions x_i and x_j, respectively [32]

$$x_q = (2q-1)\frac{W_e}{2N}, \quad q = i, j, \quad i, j = 1, 2, \ldots, N. \tag{2}$$

The phases φ_{ij} associated with imaging input i to output j are [30], [32]

$$\varphi_{ij} = \phi_1 - \frac{\pi}{2}(-1)^{i+j+N} + \frac{\pi}{4N} \times \left[i + j - i^2 - j^2 + (-1)^{i+j+N}\left(2ij - i - j - \frac{1}{2}\right)\right], \quad i, j = 1, 2, \ldots, N \tag{3}$$

with

$$\phi_1 = -\beta_0 \frac{3L_\pi}{N} - \frac{9\pi}{8N} + \frac{3\pi}{4}. \tag{4}$$

From an inspection of (3), it is easy to verify that $\varphi_{ij} = \varphi_{ji}$, owing to the symmetry of the device. An optical pulse at any of MMI coupler inputs is reproduced at the coupler outputs in the form of N self-images and distributed to the array waveguides, which have different lengths. The pulses travel different paths in the array arms and delayed copies of the pulse are then combined together by the following MMI coupler (see Fig. 4). Therefore, the impulse response of a GMZI from the input i to the output k is

$$h_{ik}(t) = \sum_{j=1}^{N} \exp\left[\mathbf{j}\left(\varphi_{ij} + \varphi_{jk} + \theta_j\right)\right] \delta\left(t - \frac{n_e L_j}{c}\right), \quad i, k = 1, 2, \ldots, N \tag{5}$$

where $\mathbf{j} = \sqrt{-1}$, $\delta(t)$ is the Dirac delta, θ_j is a constant phase shift introduced by the jth phase shifter, and c is the speed of light in vacuum; moreover, L_j is the length of the jth array arm and n_e is the corresponding (effective) refractive index. Since we are interested in OCs composed of equally spaced chips, it is necessary that the lengths L_j ($j = 1, 2 \ldots, N$) satisfy the condition

$$L_j = L_m + d_j \Delta L \quad j = 1, 2, \ldots, N \quad \text{with}$$
$$d_j \text{ integer} \in [0, 1, 2, \ldots, N-1] \text{ and } d_j \neq d_j' \text{ if } j \neq j'. \tag{6}$$

L_m is the length of a reference waveguide, which is assumed to be the shortest ($d_m = 0$), and ΔL is the minimum difference between two waveguides. Although in a general case, the lengths of the array do not increase linearly with j, it is necessary that the array arm factors d_j are all different and cover completely the interval $[0 \div N-1]$. We remark that this condition is not included in the design rules of a GMZI phasar, because in that case arbitrary values of the array arm factors d_j can be chosen, with the only requirement being that they all are different [30], [33]

The impulse response from the input i to the reference output m is

$$h_{im}(t) = \sum_{j=1}^{N} \exp\left[\mathbf{j}\left(\varphi_{ij} + \varphi_{jm} + \theta_j\right)\right] \delta\left(t - \frac{n_e L_j}{c}\right), \quad i = 1, 2, \ldots, N. \tag{7}$$

The OC at the output m is a sequence of N phase-shifted-keyed (PSK) chips with equal amplitude and different phases: the values θ_j have to be chosen so that the reference OC is constituted of chips with equal phases, i.e.,

$$\varphi_{ij} + \varphi_{jm} + \theta_j = 2\pi A_{ijm}, \quad i, j = 1, 2, \ldots, N \tag{8}$$

where A_{ijm} are integers. For a fixed input i and reference output m, the values of the phase shifters θ_j are computed from (8). We observe that in general no phase shifters are required for a GMZI multiplexer [30], [33].

If the OCs at the outputs k and k' are orthogonal, the cross-correlation function of the corresponding impulse responses is about zero

$$h_{ik}(t) \otimes h_{ik'}(t) \simeq 0, \quad i, k, k' = 1, 2, \ldots, N, \quad \text{and} \quad k \neq k'. \tag{9}$$

The transfer function $H_{ik}(f)$ from the input i to the output k can be evaluated by Fourier transforming (5), as follows:

$$H_{ik}(f) = \sum_{j=1}^{N} \exp\left[\mathbf{j}\left(\varphi_{ij} + \varphi_{jk} + \theta_j\right)\right] \exp\left(-\mathbf{j}\frac{2\pi f n_e L_j}{c}\right), \quad i, k = 1, 2, \ldots, N \tag{10}$$

and, in the frequency domain, (9) becomes

$$H_{ik}(f) H_{ik'}(f) \simeq 0, \quad i, k, k' = 1, 2, \ldots, N, \quad \text{and } k \neq k'. \tag{11}$$

This condition is always satisfied if the transfer functions $H_{ik}(f)$ are translated copies of the reference function $H_{im}(f)$

$$H_{ik}(f) = H_{im}\left(f - n\frac{c}{n_e N \Delta L}\right), \quad i, k = 1, 2, \ldots, N. \tag{12}$$

Here, n is an integer that satisfies the condition that the values corresponding to two different outputs are different, i.e.,

$$k \neq k' \quad \rightarrow \quad n \neq n'. \tag{13}$$

It is very important to note that (12) converts the requirement of the OC's orthogonality into a subband filtering condition, and following this approach, in [22] we designed an optimal full E/D as a tree of MZIs. This approach underlies the OC generation method presented in this paper and allows us to transform a multiplexer into a full E/D.

The label recognition capability depends on the ratio r between the ACP and the maximum CCP [34]. An optimal code set

is constituted of OCs with identical autocorrelation and cross-correlation functions [22], and it can be generated by translating the Fourier transform of a reference code in the frequency domain. The transfer function between the input i and the reference output m is

$$H_{im}(f)=\sum_{j=1}^{N}\exp\left(-\mathbf{j}\frac{2\pi f n_e L_j}{c}\right),\quad i=1,2,\ldots,N \tag{14}$$

where use has been made of (8), and substituting it into (12), we obtain as a result

$$H_{ik}(f)=\sum_{j=1}^{N}\exp\left(\mathbf{j}\frac{2\pi n L_j}{N\Delta L}\right)\exp\left(-\mathbf{j}\frac{2\pi f n_e L_j}{c}\right),\quad i,k=1,2,\ldots,N. \tag{15}$$

By comparing (10) and (15), it is immediately verifiable that the OCs are orthogonal if the following condition is satisfied:

$$\varphi_{ij}+\varphi_{jk}+\theta_j=\frac{2\pi n L_j}{N\Delta L}+2\pi A_{jmk},\quad i,j,k=1,2,\ldots,N \tag{16}$$

where A_{jmk} is an integer. Substituting (6) and (8) into the left-hand side (LHS) and right-hand side (RHS) of (16), respectively, we have

$$\varphi_{jk}-\varphi_{jm}-2\pi A_{ijm}=\frac{2\pi n L_m}{N\Delta L}+\frac{2\pi n d_j}{N}+2\pi A_{jmk},\quad j,k=1,2,\ldots,N \tag{17}$$

and by putting $j=m$ into the previous expression, we obtain

$$\varphi_{mk}-\varphi_{mm}=\frac{2\pi n L_m}{N\Delta L},\quad k=1,2,\ldots,N. \tag{18}$$

Finally, substituting (18) into (17), we get as result

$$\Delta\varphi_{jk}=\varphi_{jk}-\varphi_{jm}-\varphi_{mk}+\varphi_{mm}=\frac{2\pi n d_j}{N}+2\pi A'_{jmk},\quad j,k=1,2,\ldots,N \tag{19}$$

with $A'_{jmk}=A_{jmk}+A_{ijm}$. We observe that $\Delta\varphi_{jm}=0$. The phase difference can be computed from (3) as follows:

$$\begin{aligned}\Delta\varphi_{jk}&=\frac{\pi(-1)^N}{2N}\left[(-1)^{j+m}\left(j-\frac{1}{2}\right)-\left(m-\frac{1}{2}\right)\right]\\&\quad\times\left[(-1)^{k+m}\left(k-\frac{1}{2}\right)-\left(m-\frac{1}{2}\right)\right]\\&\quad-\frac{\pi(-1)^N}{2N}\left[1-(-1)^{j+m}-(-1)^{k+m}+(-1)^{j+k}\right]\\&\equiv\frac{2\pi(-1)^N}{N}A_jA_k-\frac{\pi(-1)^N}{2}A_{jk},\quad j,k=1,2,\ldots,N\end{aligned} \tag{20}$$

with

$$\begin{aligned}A_q&=\frac{1}{2}\left[(-1)^{q+m}\left(q-\frac{1}{2}\right)-\left(m-\frac{1}{2}\right)\right],\quad q=j,k\\A_{jk}&=1-(-1)^{j+m}-(-1)^{k+m}+(-1)^{j+k}.\end{aligned} \tag{21}$$

A_q is an integer, whereas A_{jk} is an integer multiple of four. Therefore, the condition of (19) can be rewritten as (22) shown at the bottom of the page, where mod indicates the modulo arithmetic operation, which has been introduced to satisfy the condition $d_j\in[0,1,2,\ldots,N-1]$. These equations constitute one of the main results of the present paper and give the design rules for a full E/D realized as a GMZI. The second equation of (22) allows us to evaluate the array factors d_j and then the lengths of the array arms L_j. The first equation of (22) gives the relative phase shifts between the OC at the reference output m and the OC at the output k. Substituting (6) into (15), we can rewrite the transfer function from the input i to the output k as

$$H_{ik}(f)=\sum_{j=1}^{N}\exp\left(\mathbf{j}\frac{2\pi n L_m}{N\Delta L}\right)\exp\left(\mathbf{j}\frac{2\pi n d_j}{N}\right)\exp\left(-\mathbf{j}\frac{2\pi f n_e L_j}{c}\right),\quad i,k=1,2,\ldots,N. \tag{23}$$

For the sake of simplicity, we can choose the reference length $L_m=N\Delta L$ so that (23) becomes

$$H_{ik}(f)=\sum_{j=1}^{N}\exp\left(\mathbf{j}\frac{2\pi n d_j}{N}\right)\exp\left(-\mathbf{j}\frac{2\pi f n_e L_j}{c}\right),\quad i,k=1,2,\ldots,N \tag{24}$$

and the phases of the OCs at the output k are multiples of $2\pi/N$; in this case, (18) reads

$$\varphi_{mk}=\varphi_{mm},\quad k=1,2,\ldots,N \tag{25}$$

and the OCs generated by the GMZI configuration coincide with those from the tree of MZIs of [22]. However, the condition $L_m=N\Delta L$ is not strictly necessary and does not affect the OCs' orthogonality. We remark that both the array arm factors d_j and the distribution of the OCs at the output k do not depend on the input i, which influences only the values of the phase shifters in (8).

To give a design example, we consider a GMZI with $N=8$ inputs/outputs, assuming that the reference output is $m=2$ and that the input port is $i=4$. From (22), we obtain the array arm factors $d_j=(7\ \ 0\ \ 6\ \ 1\ \ 5\ \ 2\ \ 4\ \ 3)$; assuming a chip interval equal to $\tau=5$ ps, the array arms lengths are $L_j=(8\ \ 1\ \ 7\ \ 2\ \ 6\ \ 3\ \ 5\ \ 4)$ mm. In addition, the values of the phase shifters, evaluated from (8), are $\theta_j=-2\phi_1-(13\ \ 29\ \ -19\ \ 29\ \ -3\ \ 13\ \ -3\ \ -19)\pi/32$. The reference code at the output $m=2$ has all phases equal to

$$\begin{aligned}n&=(-1)^N A_k=\frac{(-1)^N}{2}\left[(-1)^{k+m}\left(k-\frac{1}{2}\right)-\left(m-\frac{1}{2}\right)\right],\quad k=1,2,\ldots,N\\d_j&=A_j=\left\{\frac{1}{2}\left[(-1)^{j+m}\left(j-\frac{1}{2}\right)-\left(m-\frac{1}{2}\right)\right]\right\}\bmod N,\quad j=1,2,\ldots,N\\A'_{jmk}&=-\frac{(-1)^N}{4}A_{jk}=\frac{(-1)^N}{4}\left[-1+(-1)^{j+m}+(-1)^{k+m}-(-1)^{j+k}\right]\end{aligned} \tag{22}$$

zero, whereas the labels at the other outputs are those reported in Fig. 4: the full E/D generates $N = 8$ 8-ary PSK labels, with ACP $= 64$, maximum CCP $= 6.83$, and $r = 0.107$. The OCs of Fig. 4 coincide with those from the optimal E/D of [22].

We observe the array arm factors given by (22) do not increase monotonically with j, and to avoid crossing of the guides, it is necessary either to insert multiple U bends or to use an S configuration [33]. To avoid this drawback, we can design a GMZI with the additional requirement that $d_j = \alpha j$, with α integer. In this case, it is $m = 0$, and the second equation of (22) becomes

$$\frac{2\alpha j - \frac{1}{2}}{j - \frac{1}{2}} = (-1)^{j+m}, \quad j = 1, 2, \ldots, N \tag{26}$$

which is always satisfied for an even value of j and $\alpha = 2$. Therefore, we can design an E/D considering only even inputs, outputs, and array arms; in this case, the array arm lengths increase monotonically.

Finally, we remark that it is difficult to fabricate MMI couplers with a large number of inputs/outputs N, and therefore, the configuration of Fig. 4 allows us to generate/process only a small number of codes. However, it is easy to demonstrate that it is possible to generate OC sequences with a larger code cardinality using a tree of GMZIs with appropriate delays ΔL, following a scheme analogous to that one of [22].

II. WGR Configuration

A standard WGR multiplexer consists of N input waveguides, N output waveguides, two focusing slab waveguides, and an AWG, as depicted in Fig. 5 [35], [36]. The location of the input and output waveguides on each slab is based on the Rowland circle construction, and the length between adjacent waveguides in the grating varies by a constant ΔL [37], [38]. To design a WGR as a full E/D, we consider the transfer function between the input i and the output k

$$H_{ik}(f) = \sum_{j=1}^{N} \exp\left[-\mathbf{j}\frac{2\pi j f n_s d}{c}(\sin\theta_i + \sin\theta_o)\right] \exp\left(-\mathbf{j}\frac{2\pi f n_e j \Delta L}{c}\right), \quad i, k = 1, 2, \ldots, N. \tag{27}$$

where n_s and n_e are the effective refractive indexes of the slab and the array waveguide, respectively, d is the pitch of the AWG, and θ_i and θ_o are the diffraction angles in the input and output slabs, respectively

$$\sin\theta_i \cong i\frac{d_i}{R}, \qquad \sin\theta_o \cong k\frac{d_o}{R}. \tag{28}$$

The pitches of the input and output waveguide arrays are designated by d_i and d_o, respectively, and R is the slab focal length. Substituting (28) into (27), with the assumption $d_i = d_o$, and choosing the layout parameters such that

$$\frac{\lambda R}{n_s d d_o} = N \tag{29}$$

(27) becomes

$$H_{ik}(f) = \sum_{j=1}^{N} \exp\left[-\mathbf{j}\frac{2\pi j}{N}(i+k)\right] \times \exp\left(-\mathbf{j}\frac{2\pi f n_e j \Delta L}{c}\right), \quad i, k = 1, 2, \ldots, N. \tag{30}$$

For each input i, we define a reference output waveguide $m = N - i$ if $i \neq N$ and $m = N$ if $i = N$; the corresponding transfer function is

$$H_{im}(f) = \sum_{j=1}^{N} \exp\left(-\mathbf{j}\frac{2\pi f n_e j \Delta L}{c}\right), \quad i = 1, 2, \ldots, N \tag{31}$$

and the relative impulse response is

$$h_{im}(t) = \sum_{j=1}^{N} \delta(t - j\tau), \quad i = 1, 2, \ldots, N \tag{32}$$

where $\tau = \Delta L n_e / c$ is the chip period of the OCs, which coincides with the inverse of the free spectral range of a WGR multiplexer. The device of Fig. 5 builds the same OCs from a GMZI or a tree of MZIs; in fact, from an inspection of (30), it is easy to verify that the transfer function from the input i to the output k is a translated version of the reference function

$$H_{ik}(f) = H_{im}\left(f - \frac{i+k}{N\tau}\right), \quad i, k = 1, 2, \ldots, N. \tag{33}$$

We also remark that it is

$$H_{ik}(f) = H_{i-p,k+p}(f), \quad i, k = 1, 2, \ldots, N. \tag{34}$$

In this way, we demonstrated that a standard WGR can be designed as a full E/D that generates/processes N OCs, in an analogous way of the device described in the previous section.

Using the WGR configuration, the code cardinality can be increased up to 256 or more, since the number of the outputs of a standard WGR is not a limitation. However, the OCs generated have lengths equal to N, and therefore an increase of N would increase the label processing time at each routing node.

To avoid this drawback, we observe that the code cardinality can be increased without changing the code length if we encode labels on different wavelengths using tuneable lasers as sources of the input chips. This approach is quite similar to the wavelength-hopping time-spreading OCDMA [27], [28].

III. Multidimensional OCs

Another way to increase the code cardinality without increasing the code length is to generated multidimensional codes. In fact, if we drive two or more pulses at the same wavelength into the device inputs, we obtain N orthogonal OCs; since we can choose the inputs distribution in an arbitrary way, we can build a larger set of orthogonal photonic labels. For $n \leq N$ inputs, the code cardinality is increased up to $\binom{N}{n}$, whereas the code length remains N. The maximum number of OCs of length N that can be generated using a multidimensional configuration is $\binom{N}{N/2}$, obtained for $n = N/2$ inputs. For

instance, with $N = 8$, the code cardinality of four-dimensional OCs is 70.

We provide a simple example, considering a 2-D E/D. To generate the OCs, we send two identical pulses at the same wavelength into the device inputs i and i'. The transfer function to the output k is

$$\begin{aligned} H_k(f) &= H_{ik}(f) + H_{i'k}(f) \\ &= \sum_{j=1}^{N} \exp\left[-\mathbf{j}\frac{2\pi j}{N}(i+k)\right] \exp\left(-\mathbf{j}\frac{2\pi f n_e j \Delta L}{c}\right) \\ &\quad + \sum_{j=1}^{N} \exp\left[-\mathbf{j}\frac{2\pi j}{N}(i'+k)\right] \exp\left(-\mathbf{j}\frac{2\pi f n_e j \Delta L}{c}\right) \\ &= H_{im}\left(f - \frac{i+k}{N\tau}\right) + H_{im}\left(f - \frac{i'+k}{N\tau}\right), \\ &\quad i, i', k = 1, 2, \ldots, N \end{aligned} \tag{35}$$

where $m = N - i$ (or $m = N$ if $i = N$) is the reference output corresponding to the input i. The impulse response is

$$\begin{aligned} h_t(f) &= h_{ik}(t) + h_{i'k}(t) \\ &= \sum_{j=1}^{N} \left\{ \exp\left[-\mathbf{j}\frac{2\pi j}{N}(i+k)\right] + \exp\left[-\mathbf{j}\frac{2\pi j}{N}(i'+k)\right] \right\} \delta(t - j\tau) \\ &= \exp\left[-\mathbf{j}\frac{2\pi j}{N}\left(k + \frac{i-i'}{2}\right)\right] \cos\left(\pi j \frac{i+i'}{N}\right) \delta(t - j\tau), \\ &\quad i, i', k = 1, 2, \ldots, N \end{aligned} \tag{36}$$

so that in general the OCs have unequal amplitudes and phases. In particular, if $i - i' = N/2$, we generate OCs of length N composed only of even chip pulses with the same amplitudes.

In the present paper, we evidenced more times that the generation process of an optimal code sequence coincides with the filtering process of a multiplexer. In the case of a multidimensional E/D, each label is generated with n filters (see (35)). When a label is driven into any input ports, we measure n ACPs at the device outputs. For instance, if the label obtained at the output k is driven into the input port $i = k$, we observe two autocorrelation signals at the outputs i and i', due to the device reciprocity. For a multidimensional OC set, we can reveal an exact match measuring the simultaneous presence of two or more ACPs.

For a 2-D code set with $N = 8$, we have ACP $= 16$, and maximum CCP $= 3$ so that it is $r = 0.187$, slightly greater than monodimensional OCs.

IV. Conclusion

A recent paper [22] introduced an innovative scheme for a full E/D that generates/processes a set of N optical labels simultaneously. It was shown that it is possible to build an optimal code set, where all the labels have the same autocorrelation and cross-correlation functions, with high ACP and low maximum CCP.

The present paper shows that the code generation process is analogous to a subband filtering and that standard multiplexers like GMZIs or WGRs can be designed as full E/Ds. Design guidelines were furnished for both architectures, evidencing the analogies and the differences from standard phasars. The OCs generated by the proposed devices have cardinality N that coincides with the code lengths. To increase the number of orthogonal labels, without changing their lengths, a new concept of multidimensional E/D was introduced. If two or more identical pulses were driven at full E/D inputs, a larger set of OCs were obtained, whose cardinality depends on the number of different input distributions. The exact matching of a code label is revealed, detecting two or more ACPs. A multidimensional OC has quite the same label recognition capability of a standard OC.

Acknowledgment

The author would like to thank the anonymous reviewer, whose comments and suggestions have improved the technical writing of the paper.

References

[1] C. Cavazzoni, V. Barosco, A. D' Alessandro, A. Manzalini, S. Milani, G. Ricucci, R. Morro, R. Geerdsen, U. Hartmer, G. Lehr, U. Pauluhn, S. Wevering, D. Pendarakis, N. Wauters, R. Gigantino, J. P. Vasseur, K. Shimano, G. Monari, and A. Salvioni, "The IP/MPLS over ASON/GMPLS: Test bed of the IST project LION," *J. Lightwave Technol.*, vol. 21, pp. 2791–2903, Nov. 2003.

[2] A. Manzalini, K. Shimano, C. Cavazzoni, and A. D' Alessandro, "Architecture and functional requirements of control planes for automatic switched optical networks: Experience of the IST project LION," *IEEE Commun. Mag.*, vol. 40, pp. 60–65, Nov. 2002.

[3] R. Parthiban, R. S. Tucker, and C. Leckie, "Waveband grooming and IP aggregation in optical networks," *J. Lightwave Technol.*, vol. 21, pp. 2476–2488, Nov. 2003.

[4] S. Sánchez-López, J. Solé-Pareta, J. Comellas, J. Soldatos, G. Kylafas, and M. Jaeger, "PNNI-based control plane for automatically switched optical networks," *J. Lightwave Technol.*, vol. 21, pp. 2673–2682, Nov. 2003.

[5] A. Banerjee, J. Drake, J. Lang, B. Turner, D. Awduche, L. Berger, K. Kompella, and Y. Rekhter, "Generalized multiprotocol label switching: An overview of signaling enhancements and recovery techniques," *IEEE Commun. Mag.*, vol. 39, pp. 144–151, July 2001.

[6] A. Banerjee, J. Drake, J. P. Lang, B. Turner, K. Kompella, and Y. Rekhter, "Generalized multiprotocol label switching: An overview of routing and managements enhancements," *IEEE Commun. Mag.*, vol. 39, pp. 144–150, Jan. 2001.

[7] K. Sato, N. Yamanaka, Y. Takigawa, M. Koga, S. Okamoto, K. Shiomoto, E. Oki, and W. Imajuku, "GMPLS-based photonic multilayer router (Hikari router) architecture: An overview of traffic engineering and signaling technology," *IEEE Commun. Mag.*, vol. 40, pp. 96–101, Mar. 2002.

[8] S. Sengupta, V. Kumar, and D. Saha, "Switched optical backbone for cost-effective scalable core IP networks," *IEEE Commun. Mag.*, vol. 41, pp. 60–70, June 2003.

[9] S. Okamoto, E. Oki, K. Shimano, A. Sahara, and N. Yamanaka, "Demonstration of the highly reliable HIKARI router network based on a newly developed disjoint path selection scheme," *IEEE Commun. Mag.*, vol. 40, pp. 52–59, Nov. 2002.

[10] J. Comellas, R. Martínez, J. Prat, V. Sales, and G. Junyent, "Integrated IP/WDM routing in GMPLS-based optical networks," *IEEE Network*, pp. 22–27, Mar./Apr. 2003.

[11] A. Elwalid, D. Mitra, I. Saniee, and I. Widjaja, "Routing and protection in GMPLS networks: From shortest paths to optimized designs," *J. Lightwave Technol.*, vol. 21, pp. 2828–2838, Nov. 2003.

[12] R. Xu, Q. Gong, and P. Ye, "A novel IP with MPLS over WDM-based broad-band wavelength switched IP network," *J. Lightwave Technol.*, vol. 19, pp. 596–602, May 2001.

[13] K. G. Vlachos, I. T. Monroy, A. M. J. Koonen, C. Peucheret, and P. Jeppesen, "STOLAS: Switching technologies for optically labeled signals," *IEEE Commun. Mag.*, pp. 9–15, Nov. 2003.

[14] K. H. Liu, *IP Over WDM*. West Sussex, U.K.: Wiley, 2003.

[15] K.-I. Kitayama and M. Murata, "Versatile optical code-based MPLS for circuit, burst, and packet switchings," *J. Lightwave Technol.*, vol. 21, pp. 2753–2764, Nov. 2003.

[16] K.-I. Kitayama and N. Wada, "Photonic IP routing," *J. Lightwave Technol.*, vol. 11, pp. 1689–1691, Dec. 1999.

[17] M. Murata and K.-I. Kitayama, "A perspective on photonic multiprotocol label switching," *IEEE Network*, pp. 56–63, July/Aug. 2001.
[18] K.-I. Kitayama, N. Wada, and H. Sotobayashi, "Architectural considerations for photonic IP router based upon optical code correlation," *J. Lightwave Technol.*, vol. 18, pp. 1834–1844, Dec. 2000.
[19] N. Wada and K.-I. Kitayama, "Photonic IP routing using optical codes: 10 Gbit/s optical packet transfer experiment," in *Proc. Optical Fiber Communication Conf. (OFC)*, vol. 2, Baltimore, MD, 2000, WM51-1, pp. 362–364.
[20] K.-I. Kitayama and M. Murata, "Photonic access node using optical-code based label processing and its applications to optical data networking," *J. Lightwave Technol.*, vol. 19, pp. 1401–1415, Oct. 2001.
[21] N. Wada, W. Chujo, and K.-I. Kitayama, "1.28 Tbit/s (160 Gbit/s $\times$ 8 wavelengths) throughput variable length packet switching using optical code based label switch," in *Proc. 27th Eur. Conf. Opt. Comm. (ECOC)*, vol. 6, Amsterdam, The Netherlands, 2001, pp. 62–63.
[22] G. Cincotti, "Full optical encoders/decoders for photonic IP routers," *J. Lightwave Technol.*, vol. 22, pp. 337–342, Feb. 2004.
[23] ——, "," PCT Patent Application No. PCT/IT03/000 879, Dec. 30, 2003.
[24] R. A. Griffin, D. D. Sampson, and D. A. Jackson, "Optical phase coding for code-divison multiple access networks," *IEEE Photon. Technol. Lett.*, vol. 4, pp. 1401–1404, Dec. 1992.
[25] ——, "Demonstration of data transmission using coherent correlation to reconstruct a coded pulse sequence," *IEEE Photon. Technol. Lett.*, vol. 4, pp. 513–515, May 1992.
[26] M. Vetterli and C. Herley, "Wavelets and filter banks: Theory and design," *IEEE Trans. Signal Processing*, vol. 40, pp. 2207–2232, Sept. 1992.
[27] S. Yegnanarayanan, A. S. Bhushan, and B. Jalali, "Fast wavelength-hopping time-spreading encoding/decoding for optical CDMA," *IEEE Photon. Technol. Lett.*, vol. 12, pp. 573–575, May 2000.
[28] K. Takiguchi, T. Shibata, and M. Itoh, "Encoder/decoder on planar lightwave circuit for time-spreading/wavelength-hopping optical CDMA," *Electron. Lett.*, vol. 38, no. 10, pp. 469–470, 2002.
[29] C. K. Madsen and J. H. Zhao, *Optical Filter Design and Analysis. A Signal Processing Approach*. New York: Wiley, 1999.
[30] M. R. Paiam and R. I. MacDonald, "Design of phased-array wavelength division multiplexers using multimode interference couplers," *Appl. Opt.*, vol. 36, no. 21, pp. 5097–5108, 1997.
[31] L. B. Soldano, F. B. Veerman, M. K. Smit, B. H. Verbeek, A. H. Dubost, and E. C. M. Pennings, "Planar monomode optical couplers based on multimode interference effects," *J. Lightwave Technol.*, vol. 10, pp. 1843–1850, Dec. 1992.
[32] M. Bachmann, P. A. Besse, and H. Melchior, "General self-imaging properties in $N \times N$ multimode interference couplers including phase relations," *Appl. Opt.*, vol. 33, no. 18, pp. 3905–3911, 1994.
[33] P. A. Besse, M. Bachmann, C. Nadler, and H. Melchior, "The integrated prism interpretation of multileg Mach–Zehnder interferometers based on multimode interference couplers," *Opt. Quantum Electron.*, vol. 27, pp. 909–920, 1995.
[34] S. W. Lee and D. H. Green, "Coding for coherent optical CDMA networks," *IEE Proc. Commun.*, vol. 145, no. 3, pp. 117–125, 1998.
[35] C. Dragone, "An $N \times N$ optical multiplexer using a planar arrangement of two star couplers," *IEEE Photon. Technol. Lett.*, vol. 3, pp. 812–815, Sept. 1991.
[36] H. Takahashi, K. Oda, H. Toba, and Y. Inoue, "Transmission characteristics of arrayed waveguide $N \times N$ wavelength multiplexer ," *J. Lightwave Technol.*, vol. 13, pp. 447–455, Mar. 1995.
[37] C. Dragone, C. A. Edwards, and R. C. Kistler, "Integrated optics $N \times N$ multiplexer on silicon," *IEEE Photon. Technol. Lett.*, vol. 3, pp. 896–899, Oct. 1991.
[38] R. Adar, C. H. henry, C. Dragone, R. C. Kistler, and M. A. Milbrodt, "Broad-band array multiplexers made with silica waveguides on silicon," *J. Lightwave Technol.*, vol. 11, pp. 212–219, Feb. 1993.

Gabriella Cincotti (M'01) was born in Naples, Italy, in 1966. She received the Laurea (M.Sc. equivalent) degree in electronic engineering (*cum laude*) from "La Sapienza" University of Rome, Rome, Italy, in 1992.

She was a Project Engineer at the microwave laboratory of ALENIA, Aeritalia & Selenia S.p.A., Rome, Italy, from 1992 to 1994 and joined the Department of Electronic Engineering of University of "Roma Tre," Rome, Italy, as an Assistant Professor in October 1994. Her ongoing research areas include passive optical devices, optical filters, wavelength demultiplexing, encoders/decoders and polarizing devices, and her research results have been recorded in more than 50 refereed papers and summarized in nearly 20 conference and symposium presentations.

Ms. Cincotti is a Member of the IEEE Lasers & Electro-Optics Society (LEOS), the Optical Society of America (OSA), the Consorzio Nazionale Interuniversitario per le Telecomunicazioni (CNIT), and the National Institute for the Physics of the Matter (INFM) Unity Roma 3, Rome, Italy.